Journal of Structural Engineering. Submitted May 24, 2011; accepted September 6, 2012;
posted ahead of print September 8, 2012. doi:10.1061/(ASCE)ST.1943-541X.0000718

Retracted: Self-centering prestressed concrete beam-column connections with web friction devices

Tong Guo[1]; Liang-long Song[2]; Richard Sause[3]; and Cheng Chen[4]

Abstract: A novel self-centering prestressed concrete (SCPC) beam-column connection with a web friction device has been developed to reduce the residual deformation and damage of precast concrete frames under earthquake loading. Precast concrete beams and columns are assembled and prestressed together using unbonded post-tensioned tendons. Under cyclic loading, gap opening and closing occur at the beam-column interfaces. Jackets at the beam ends and steel plates embedded in the columns protect the concrete from crushing at the beam-column interfaces. Friction devices located near the beam-column interfaces provide energy dissipation. To evaluate the seismic behavior of the SCPC connection, fourteen cyclic loading tests were conducted on four full-scale specimens. Results show that the SCPC connection has desirable self-centering behavior with energy dissipation. The specimens underwent a relative rotation of 0.038rad without significant damage to the beams or columns. Analytical models are developed for the SCPC connection. Good agreement is observed between analytical and experimental results. Future work is suggested based on the experimental study to improve the SCPC connection.

Author keywords: Self-centering; Prestressed concrete frame; Beam-column connection; Cyclic

[1] Professor, Key Laboratory of Concrete and Prestressed Concrete Structures of the Ministry of Education, Southeast Univ., Nanjing, P.R.China,210096 (corresponding author); formerly, Visiting Research Scientist, ATLSS Center; E-mail: guotong77@gmail.com

[2] Postgraduate Researcher, School of Civil Engineering, Southeast Univ., Nanjing, P.R.China, 210096. E-mail: seusongll@gmail.com

[3] Joseph T. Stuart Professor of Structural Engineering and Director, ATLSS Center, Dept. of Civil and Environmental Engineering, Lehigh Univ., Bethlehem, PA 18015. E-mail: rs0c@lehigh.edu

[4] Assistant Professor, School of Engineering, San Francisco State University, San Francisco, CA,USA, 94132. E-mail: chcsfsu@sfsu.edu

Journal of Structural Engineering. Submitted May 24, 2011; accepted September 6, 2012;
posted ahead of print September 8, 2012. doi:10.1061/(ASCE)ST.1943-541X.0000718

loading; Web friction device.

Introduction

Precast concrete (PC) moment-resisting frames (MRFs) are cost-efficient building structures. However, the use of PC-MRFs has been limited in seismic regions by concerns about their performance during earthquakes. In recent decades, extensive research has been devoted to improve the performance of PC-MRFs, so as to achieve performance similar to or better than cast-in-situ reinforced concrete (RC) MRFs (Korkmaza and Tankutb 2005; Dolan et al. 1987; Sucuoglu 1995; Martin and Perry 2004). However, both PC-MRFs and RC-MRFs can have significant residual drift after earthquakes, and damage to the beam-column connections can require expensive post-earthquake repairs. To reduce the residual drift, unbonded post-tensioned PC-MRFs have been investigated (Liu et al. 2007; Englekirk 2002; fib Bulletin 27 2003; El-Sheikh et al. 1999). One concern regarding post-tensioned PC-MRFs is the low energy dissipation under cyclic loading (Priestley and MacRae 1996). Supplemental passive energy dissipation elements may be required. Morgen and Kurama (2008) used friction devices at the beam ends to increase the energy dissipation. However, friction devices which are located at the top and bottom surfaces of the beams may interfere with the floor slab. Another concern is the concrete local compression failure (spalling or crushing) that may occur at the beam-column interfaces under cyclic loading, resulting in a loss of PT forces and self-centering (SC) behavior.

Post-tensioned steel MRFs have been investigated. Energy dissipation in these systems is achieved from energy dissipation elements instead of inelastic deformation of the main structural elements. Energy dissipation elements including top-and-seat angles (Garlock 2002), steel bars (Christopoulos 2002), reduced flange reinforcing plates (Chou et al. 2005) and other yielding elements (Chou and Lai 2009), as well as friction devices (Rojas et al. 2005; Wolski et al. 2009; Lin et al. 2009) have been studied.

Journal of Structural Engineering. Submitted May 24, 2011; accepted September 6, 2012;
posted ahead of print September 8, 2012. doi:10.1061/(ASCE)ST.1943-541X.0000718

Compared with PC-MRFs, the advantages of steel SC-MRFs are: local compression failure at the beam-column interface can be avoided. However, buckling in beam webs and flanges may occur in steel MRFs, and steel MRFs may have higher material costs.

Motivated by this prior research, a self-centering prestressed concrete (SCPC) beam-column connection with a web friction device is proposed and investigated in this study. The SCPC connection is intended to combine the advantages of post-tensioned PC-MRFs and steel SC-MRFs. This paper presents an experimental and analytical study on the behavior of the SCPC connection under cyclic loading.

Analysis of SCPC connection with web friction device

Connection description

Fig.1(a) shows a typical SCPC beam-column connection from the present study, where unbonded PT tendons compress the precast concrete beam to the column. Steel jackets, as shown in Fig.1(b), are fabricated and the beam ends are cast inside these jackets; the jackets protect the concrete at the beam-column interfaces from spalling and crushing. One end of each outer steel channel is welded to a steel plate that is embedded in the column. Sandwiched between the outer channels and the steel jacket are two friction plates (i.e., brass plates), which are attached to the two inner surfaces of the steel channels. High strength friction bolts with washers compress the friction device together and produce controlled normal forces on the friction surfaces. The channels are welded to the steel plate (embedded in the column) after the friction bolts are tightened, so that the bolt forces developed during tightening of the bolts are not resisted by bending of the channels. In addition, the shape of the channels reduces the tendency for shrinkage of the welds to decrease the normal forces on the friction surfaces. The diameter of the holes through the steel jacket and beam is much larger than that of the friction bolts to accommodate the relative motion of friction bolts when the beam rotates relative to the column, as shown

Journal of Structural Engineering. Submitted May 24, 2011; accepted September 6, 2012;
posted ahead of print September 8, 2012. doi:10.1061/(ASCE)ST.1943-541X.0000718

in Fig.1(c). Because the friction device is located near the beam mid depth, there is no interference between the friction device and the floor slab.

Forces at beam end

The conceptual behavior of the SCPC connection under negative bending moment is derived from the free body diagram in Fig.2. Under external loads, the reaction forces at the beam end include: (1) axial reaction forces at the upper and lower centers of rotation, N_t and N_b; (2) the friction force of the web friction device, F_f, which can be expressed (assuming Coulomb friction) as,

$$F_f = 2\mu_f N_f \tag{1}$$

and; (3) friction forces at two centers of rotation, V_t and V_b written as,

$$\begin{cases} V_t = \mu \cdot N_t \\ V_b = \mu \cdot N_b \end{cases} \tag{2}$$

where μ_f is the coefficient of friction between the friction plate and the steel jacket; N_f is the normal force on the friction surfaces, assumed to be equal to the sum of friction bolt forces. N_f is determined from the energy dissipation required for the connection. The hysteretic energy dissipation ratio, β_E, can be used to quantify the required energy dissipation. β_E is the ratio of the energy dissipation of the system to the energy dissipation of a bilinear elastic-plastic system with the same force capacity (Seo and Sause, 2005). To maintain self-centering, β_E can range from 0 to 0.5. ACI Innovation Task Group 1 (2001) recommends that β_E should be no less than 0.125. Seo and Sause (2005) show that β_E values greater than 0.25 result in drift demands under earthquake loading similar to those of conventional earthquake-resistant systems.

The axial reaction forces at the beam end, from equilibrium, are,

$$N_t + N_b = P + F_f \cdot \cos\alpha \tag{3}$$

where $F_f \cdot \cos\alpha$ is the horizontal component of F_f; α is the angle between F_f and the horizontal plane; and P is the resultant force of all tendons forces.

Journal of Structural Engineering. Submitted May 24, 2011; accepted September 6, 2012;
posted ahead of print September 8, 2012. doi:10.1061/(ASCE)ST.1943-541X.0000718

The connection moment (at the beam-column interface) when the connection is open (after gap opening) under negative moment, M, can be expressed in terms of P and F_f. In this case, N_t=0, since the top of the beam is not in contact with the column, and the center of rotation is at the bottom of the beam. M has two parts, M_{PT} and M_{Ff}, as shown in Eq. (4). Assuming F_f is applied at the centroid of the bolts of the friction device, and the distance between F_f and center of rotation is r, M can be expressed as

$$M = M_{PT} + M_{Ff} = \sum_{i=1}^{n} T_i d_i + F_f \cdot r \tag{4}$$

where T_i is the tensile force of the ith tendon; $P = \sum_{i=1}^{n} T_i$; and d_i is the distance from T_i to the center of rotation. Under positive bending, the result is similar, except that the center of rotation is at the top of the beam.

The shear forces at the beam end, V_t and V_b, due to friction at the beam-column interface should be larger than the maximum shear force demand. Previous studies (Wolski et al 2009; Garlock et al 2005; Chou et al 2006; Chou et al 2009; Christopoulos et al 2002) have shown the adequacy of these friction forces. The friction forces in the friction device may also contribute to the shear capacity.

Conceptual $M - \theta_r$ relationship

The conceptual moment-relative rotation (M-θ_r) behavior of the SCPC connection under cyclic loading is illustrated in Fig.3 (Wolski et al. 2009), where M is the moment at the beam-column interface (total moment acting on the column from the connection) and θ_r is the relative rotation between the beam end and the column. The beam-column interface is in complete contact until the applied external moment exceeds the sum of M_{PT} and M_{Ff}, which is defined as event 1. The moment at event 1 in Fig.3 is referred to as the imminent gap-opening moment M_{IGO} (Wolski et al. 2009), which can be calculated as

$$M_{IGO} = \sum_{i=1}^{n} T_{0i} d_i + F_{f0} \cdot r \tag{5}$$

Journal of Structural Engineering. Submitted May 24, 2011; accepted September 6, 2012;
posted ahead of print September 8, 2012. doi:10.1061/(ASCE)ST.1943-541X.0000718

where T_{0i} is the initial PT force of the ith tendon and F_{f0} is the maximum static friction force.

After event 1, gap-opening occurs and the PT tendons elongate as θ_r increases. The gap between the column and the beam is expressed as

$$\Delta_{gap} = \theta_r \cdot h \tag{6}$$

where h is the distance between the two centers of rotation at the top and the bottom of the beam. After event 1, the friction force resultant F_f is assumed to remain constant and located at the centroid of friction bolts. If loading continues, yielding of the tendons can occur, and is defined as event 3. At unloading (defined as event 2) the moment due to friction changes direction due to a reversal of the friction force. During the reversal of the friction force (between event 2 and event 5), θ_r remains constant. As unloading continues, θ_r decreases to zero from event 5 to event 6, when the gap closes, with N_t equal to zero. Thereafter, M reduces to zero at event 7. It is worth noting that the M-θ_r behavior of the SCPC connection under cyclic loads is usually symmetric under positive and negative moments, since the friction device is symmetric to the centroidal axis of the beam.

After gap-opening occurs, the $M-\theta_r$ stiffness is provided by the PT tendons since the friction force is relatively constant. The slope of the line from event 1 to event 2 in Fig.3 is determined by the depth of the beam, the axial stiffness and arrangement of the PT tendons, and the axial stiffness of the beam.

Cyclic load tests on SCPC connections with web friction devices

Test specimens

To evaluate the behavior of the proposed SCPC connection under cyclic loading, four full scale specimens were fabricated, assembled, and tested in the Key Laboratory of Concrete and Prestressed Concrete Structures of the Ministry of Education at Southeast University. Fourteen tests were conducted on the four specimens. The length of the beams and the columns of these test specimens was 1.5m. The

Journal of Structural Engineering. Submitted May 24, 2011; accepted September 6, 2012;
posted ahead of print September 8, 2012. doi:10.1061/(ASCE)ST.1943-541X.0000718

cross sections of the beams and the columns were 300×500 mm and 400×400 mm, respectively. Fig.4(a) shows the details of specimen SCPC1, as an example, in which four tendon ducts with a diameter of 40 mm were cast into the beam and the column. A steel jacket was shop-fabricated and one end of the beam was cast inside the jacket. Two 400×1,000×8 mm steel plates were embedded in the concrete column. Two shim plates were welded to these steel plates at the beam-column interface, as shown in Fig.4(a), to ensure good contact between the beam and the column. Shear studs were welded to the inner surfaces of the steel jacket and steel plates to provide anchorage of the steel plates to the concrete. The thickness of the embedded steel plates, shim plates and steel jacket was 8 mm. Considering that the concrete at the beam ends in contact with the column will dilate (expand laterally) under high stresses at the beam-column interface, four spiral hoops were used at the beam end to confine the concrete. The spiral hoops had an outer diameter of 125 mm and the diameter of the spiral reinforcement was 6mm. Six bolt ducts, running perpendicular to the beam axis, were built into the beam, as shown in Fig.4(b). Two friction plates (i.e., 2 mm thick brass plates) were sandwiched between the two steel channels and the steel jacket. Friction bolts passed through the channels, brass friction plates, and beam. One end of each steel channel was welded to the embedded steel plate in the column. The six friction bolts installed in the bolt ducts had a diameter of 18mm. The bolt ducts had a diameter of 50 mm to accommodate the relative movement of the bolts and the beam after gap opening. When the beam and the column were assembled, post-tensioning forces were applied to the tendons and friction bolts via a hydraulic jack and a torque wrench, respectively. A strain gauge was used on each friction bolt to control the pretension forces.

Specimen SCPC2 has the same dimensions and reinforcement arrangement as SCPC1, but has no steel jacket, no friction device, and no embedded steel plates in the column. Specimen XJ1 was a monolithic cast-in-place beam-column connection with same dimensions as SCPC1. Accordingly, there

Journal of Structural Engineering. Submitted May 24, 2011; accepted September 6, 2012;
posted ahead of print September 8, 2012. doi:10.1061/(ASCE)ST.1943-541X.0000718

were no steel jackets, no friction device, and no steel plates in specimen XJ1. Specimen SCPC3 was designed to be the same as specimen SCPC1, but without the spiral hoops.

Test setup and instrumentation

The test setup and the assembly are illustrated in Fig.5(a) and Fig.5(b). The tests focused on the behavior at the beam-column interface and the friction device, rather than on the remainder of the beam, the column, and the column panel zone. The test setup in this study was similar to those used by Morgen and Kurama (2004) and Wolski et al (2009). Fully reversing cyclic loads were applied to the beam end with a loading rate of about 2 mm/s for all specimens and an axial load of 534.4 kN was applied on the column. Due to the limited length of the beams in the test specimens (i.e., 1.5 m), the increase in strain in the tendons was significant as gap opening at the beam-column interface occurs. To prevent premature yielding of the tendons, an auxiliary beam with a length of 1.5 m was added at the other side of the specimen, as shown in Fig.5 (a). The resulting effective length of the tendons (i.e., the sum of the lengths of the two beams, the width of the column, the shim plates and the length of the force transducer) was 3.6 m.

Four force transducers at the beam end measured the forces in the tendons, as shown in Fig.5(c). One displacement transducer measured the vertical displacement at the beam end. The relative rotation between the beam and column was obtained from two displacement transducers located at the top and bottom of the beam at the beam-column interface (Fig.5(c)), where $\theta_r = (\Delta_{H1} - \Delta_{H2})/D$, Δ_{H1} and Δ_{H2} are the displacements from the displacement transducers, respectively, and D is the distance between them (i.e., 610 mm). Resistance strain gauges measured the strains in the steel jacket and the friction bolts.

Material properties

The mean cubic compressive strength of the concrete was 53.3 MPa. The nominal diameter of the tendons

Journal of Structural Engineering. Submitted May 24, 2011; accepted September 6, 2012;
posted ahead of print September 8, 2012. doi:10.1061/(ASCE)ST.1943-541X.0000718

was 15.2mm, corresponding to a cross-sectional area of 140 mm^2. The tendons had a modulus of elasticity (E_{st}) of 1.95×10^5 MPa and a mean yield strength of 1,498 MPa. The coefficient of friction between the brass and steel was around 0.3. The steel plates were Q235 steel with a nominal yield strength of 235 MPa (GB 50010-2002 2002). The longitudinal reinforcing bars were HRB335 steel with a nominal yield strength of 335 MPa, and the hoops, cross ties, and spiral hoops were HPB235 steel with a nominal yield strength of 235 MPa (GB 50010-2002 2002).

Test matrix

Fourteen tests were performed on the four specimens. Table 1 summarizes the parameters and characteristics of these tests, where F_0 denotes the sum of the tendon forces of the four tendons after jacking, R_0 is the initial stress of each tendon normalized by the yield stress of the tendon (i.e., 1,498 MPa), and N_0 denotes the sum of the six friction bolt forces. Since there were no steel jackets in specimens XJ1 and SCPC2, concrete spalling and crushing were observed in early stages of these tests, and only one test was conducted on each of these two specimens. The steel jackets at the beam ends and the steel plates in the column prevented significant damage to specimens SCPC1 and SCPC3, which enabled a number of tests with different parameters to be conducted on these specimens.

Test 1 was a trial test to validate the measurement system. Tests 2, 3, 4, and 5 investigated the hysteretic behavior of the specimen with different levels of friction force. Test 6 was intended to study the relationship between tendon force and relative rotation. Different levels of friction bolt force and higher tendon forces were used in Tests 7, 8, and 9, to evaluate the influence of the friction bolt force on the self-centering behavior. Test 10 was intended to obtain the stiffness and energy dissipation of the specimen without the friction device. Specimen SCPC2 did not have a steel jacket or friction device, and Test 11A was conducted to illustrate the effect of the steel jacket and friction device. The connection

Journal of Structural Engineering. Submitted May 24, 2011; accepted September 6, 2012;
posted ahead of print September 8, 2012. doi:10.1061/(ASCE)ST.1943-541X.0000718

studied in Test 11A was investigated in previous research (e.g., El-Sheikh et al. 1999; Liu et al. 2007). Little dissipation capacity and significant spalling of the cover concrete was expected. Specimen XJ1 in Test 12 was a monolithic cast-in-place beam-column connection. Test 13 was conducted to analyze the stress distribution on the steel jacket. In Test 14, spiral hoops were omitted to investigate the necessity of these hoops.

The tests were conducted under displacement control using θ_r as the control variable. Note that the tests mainly focused on the behavior of the SCPC connection under demands from an earthquake similar to the Design Basis Earthquake (DBE) in a region of high seismicity in the US (FEMA 2003). Rojas et al. (2005) showed that post-tensioned steel MRFs with friction devices in the connections have a mean connection relative rotation of approximately 0.02 rad under the DBE, so 0.02 rad was the target rotation for most of the tests. Wolski et al. (2007) examined seismic response analysis results by Rojas (2003) for post-tensioned steel MRFs with friction devices under DBE ground motions, and estimated the probability that the connection relative rotation would exceed 0.035 rad under the DBE is less than 1%. Therefore, the target rotation for Test 14 was 0.035 rad. Test 14 was stopped after a maximum rotation of 0.038 rad, because the friction bolts began to bear against the ducts in the beams. To investigate the behavior of the connection under larger rotations, Test 11A was pushed to 0.053 rad. One cycle was conducted for each displacement level.

Experimental results and discussion

Hysteretic behavior

The hysteretic behavior of specimen SCPC1 in Test 2 is shown in Fig. 6(a) and Fig. 6(b), where the hysteresis loops are observed to have a double-flag shape. When the applied load reached 67 kN, imminent gap-opening occurred. The initial stiffness was 6,820 kN/m. After gap-opening, the stiffness

Journal of Structural Engineering. Submitted May 24, 2011; accepted September 6, 2012;
posted ahead of print September 8, 2012. doi:10.1061/(ASCE)ST.1943-541X.0000718

decreased to 1,420 kN/m. As mentioned earlier, the stiffness after gap opening is controlled by the depth of the beam, the axial stiffness and arrangement of the PT tendons, and the axial stiffness of the beam. The force in the friction device remains nearly constant, so the friction device does not contribute significantly to the post-gap-opening stiffness. A slight stiffness reduction was observed upon unloading due to the flexibility of the steel channels. When the load reached zero, the opening at the beam-column interface closed due to the PT forces in the tendons. After the test, a small residual displacement of 1.3 mm was observed at the beam end. No local yielding was observed in the steel jacket.

The influence of the friction bolt forces on the energy dissipation was demonstrated through Test 4, in which low friction bolt forces were used (i.e., 7.5 kN for each bolt). As shown in Fig. 7(a) and Fig. 7 (b), the hysteresis loops are narrow with less energy dissipation, compared with the loops in Test 2. When there is no friction bolt force, as shown in Fig. 7(c) and Fig. 7 (d) (i.e., from Test 10), the hysteresis loops are very narrow, and there is almost no energy dissipation.

In Test 5, the friction bolt force was increased to 30 kN. As shown in Fig. 6(c) and Fig. 6(d), the hysteresis loops are much wider than those from Test 2. When the applied load reached 86 kN, gap-opening occurred at the beam-column interface. The initial stiffness was 7,050 kN/m. The post-gap-opening stiffness was about 1,680 kN/m. After Test 5, the residual displacement was 3.3 mm.

Influence of tendon force

In Tests 7, 8 and 9, the tendon forces were higher than those in the previous tests. Figs. 8(a) and 8(b) present the hysteretic behavior of the specimen during Test 9. Compared with the behavior during Test 5, which had lower tendon forces and the same friction bolt forces, the initial stiffness of the connection in Test 9 increased to 10,700 kN/m, and imminent gap-opening was at a load of 104 kN. After the test, the residual displacement was 0.5 mm, which was smaller than that in Test 5 (i.e., 3.3 mm). The width of the

Journal of Structural Engineering. Submitted May 24, 2011; accepted September 6, 2012;
posted ahead of print September 8, 2012. doi:10.1061/(ASCE)ST.1943-541X.0000718

hysteresis loops and the total energy dissipation in Test 9 are similar to those in Test 5, since the two tests had the same friction bolt forces. Therefore, the tendon forces affect mainly the initial stiffness and the imminent gap-opening moment. This observation is further confirmed by comparing the results of Test 3 and Test 8, as shown in Fig. 8(c), and by comparing the results of Test 4 and Test 7, as shown in Fig. 8(d).

Relationship of tendon force and relative rotation

Test 6 was intended to investigate the relationship between the tendon force and relative rotation. As shown in Fig. 9(a) and Fig. 9(b), the tendon force changes almost linearly with relative rotation. Note that to avoid the possibility of tendon failure in the laboratory, the tendon stresses were kept below the yield strength of the tendons, so that all tendons performed elastically. However, the relationship between the tendon force and relative rotation is asymmetric under cyclic loads, due to the difference in the distance from the tendon to the center of rotation under positive and negative loading. In addition, slim hysteresis loops were observed, which means tendon forces at the same displacement were different during loading and unloading. This result may be from the change in friction force direction (in the friction device) during loading and unloading. Also, due to construction errors, the positions of the four tendons were asymmetric. For example, the distance from tendon PT1 to the bottom of the beam was 7 cm, while the distance from tendon PT2 to the top of the beam was 11 cm.

When the specimen without a friction device was tested (in Test 10), the relationship between tendon force and relative rotation has a very thin hysteresis loop, as shown in Fig. 9(c) and Fig. 9(d). However, in this case, the specimen did not have any significant energy dissipation.

Behavior of specimens without steel jacket and friction device

Fig.10 shows the behavior of the specimen without a steel jacket or friction device from Test 11A. This specimen was a typical post-tensioned precast concrete beam-column connection similar to those studied

Journal of Structural Engineering. Submitted May 24, 2011; accepted September 6, 2012;
posted ahead of print September 8, 2012. doi:10.1061/(ASCE)ST.1943-541X.0000718

by El-Sheikh et al. (1999). As shown in Fig. 10, the hysteretic loops were S-shaped with very little energy dissipation. During the test, the total tendon force decreased from 453 kN to 339 kN mainly due to damage to the concrete at the beam end. The residual displacement after the test was small (i.e., 4.8 mm) showing that this kind of specimen also has self-centering behavior.

Strain measurements on steel jacket

In Test 13, strains on the steel jacket were measured. As shown in Fig. 5(c), there were 10 strain gauges along the midline of the jacket on the top surface of the beam. These strain gauges have a spacing of 5 cm, and are labeled from gauge 1 to gauge 10 (from the beam-column interface towards the far end of the jacket). There were four full load cycles in Test 13, and Fig. 11(a) shows the strains during the upward loading in the fourth cycle. It is observed that the strain increments for gauge 1 were significant as the vertical load increased, and the strain increments did not increase linearly with the load increment. The strain increments were not very large for gauge 2 to gauge 10. Therefore, the local compression strains in the steel jacket were most significant within a distance of 5 cm away from the beam-column interface.

The strain-force relationships in the first and fourth load cycles are illustrated in Fig. 11(b). In the smaller load cycle (Cycle 1), the strain-load response is almost elastic; while in the larger load cycle (Cycle 4), the strain-load response is hysteretic. The maximum strain was 1058 με, which is less than the yield strain of the steel plate; therefore, the inelastic deformation was mainly in the adjacent concrete.

Hysteretic behavior of specimen SCPC3 (without spiral hoops)

Test 14 was conducted on specimen SCPC3 to investigate the necessity of the spiral hoops. A steel jacket was used at the beam end. More load cycles were applied in this test (i.e., 6 load cycles) and the largest positive and negative rotations were 0.035 and -0.038 rad. Fig.12 shows the hysteretic behavior during Test 14, and it appears that after each load cycle the imminent gap-opening moment becomes smaller

Journal of Structural Engineering. Submitted May 24, 2011; accepted September 6, 2012;
posted ahead of print September 8, 2012. doi:10.1061/(ASCE)ST.1943-541X.0000718

upon reloading, which appears to be from permanent inelastic compressive deformation of the concrete. Without confinement from the spiral hoops, permanent inelastic deformation occurred earlier than in the specimens with spiral hoops, and this resulted in the loss of tendon forces. However, the loss of tendon forces was small. In the last load cycle, there was a rise in the F - Δ and the M - θ_r curves, caused by the bearing of the friction bolts against the ducts in the beam. A similar bolt bearing phenomenon was reported previously by Wolski et al. (2009). No significant damage was observed in the beam or column after the test.

Failure modes

In Test 1 (the trial test), the embedded steel plates were anchored to the column using shear studs. It was observed that one steel plate separated from the concrete, indicating that the anchorage was not sufficient. This resulted in the synchronous rotation of the steel channels and steel plates towards the steel jackets, and led to a loss of energy dissipation in the connection. Therefore, in the following tests, two steel plates were added to the column, as shown in Fig. 13(a). These two plates connected the original two embedded steel plates through welds, to transfer the friction forces from the channels. An improved anchorage detail is needed, and one possibility is shown in Fig. 13(b), where the steel plates are directly welded to the longitudinal reinforcement or stirrups in the column. These welds would be made in the precast plant before the concrete is cast.

The failure mode of the monolithic cast-in-place specimen XJ1 is shown in Fig. 14(a), where shear cracking developed in the plastic hinge region at the beam end. Significant concrete spalling and crushing was observed at the top and bottom of the beam under cyclic loads. The photographs in Fig. 14 were taken at the end of the test with the load on the beam end removed. The hysteretic behavior of specimen XJ1 is not presented because the displacement transducers which measured the specimen deformation

Journal of Structural Engineering. Submitted May 24, 2011; accepted September 6, 2012;
posted ahead of print September 8, 2012. doi:10.1061/(ASCE)ST.1943-541X.0000718

malfunctioned during the test. However, the hysteretic behavior of many similar cast-in-place specimens can be found in the literature, where large residual deformations are often observed.

Compared with specimen XJ1, the damage of specimen SCPC2 in Test 11A was less severe, as shown in Fig.14(b), where only local concrete crushing and spalling were observed at the top and bottom of the beam. The relative rotation in this test ranged from -0.053 rad to +0.048 rad with a residual deformation of 0.0002 rad at the end of the test. After the tests on specimen SCPC1 and SCPC3, no significant damage were observed in the specimens except minor cracks in the welds at the ends of the channels, as shown in Fig.14(c). In Test 9, the relative rotation ranged from -0.024 rad to +0.026 rad with a residual deformation of 0.0004 rad at the end of the test.

Comparison of analytical and experimental results

Unlike the beam-column connections of a multi-bay frame, in which PT tendons are not bonded to the beams at any location within the beam span (i.e., they are anchored at the exterior columns), the tendons in the test specimens were attached to the beams at anchorages at the beam ends, as shown in Fig.15. In this case, each tendon has a different elongation after connection gap opening. The deformation of tendon i is $\Delta_{si} = \theta_r \cdot d_i$, where d_i is the distance from the ith tendon to the center of rotation.

As gap opening occurs at the beam-column interface, the tensile force in the ith tendon is

$$T_i = T_{i0} + k_{si}\left(\Delta_{si} - \delta_b\right) = T_{i0} + k_{si}\left(d_i - \frac{\sum_{i=1}^{n}\left(k_{si}d_i\right)}{\sum_{i=1}^{n}k_{si} + k_b}\right)\theta_r \tag{7}$$

where δ_b is the compressive deformation of the beam, and k_b and k_{si} are the axial stiffness of the beam and the ith tendon. The tendon contribution to M_{PT} can be expressed as

Journal of Structural Engineering. Submitted May 24, 2011; accepted September 6, 2012;
posted ahead of print September 8, 2012. doi:10.1061/(ASCE)ST.1943-541X.0000718

$$M_{PT} = \sum_{i=1}^{n}\left(T_{i0}d_i\right) + \sum_{i=1}^{n}\left[d_i k_{si}\left(d_i - \frac{\sum_{i=1}^{n}\left(k_{si}d_i\right)}{\sum_{i=1}^{n}k_{si} + k_b}\right)\right]\theta_r = \sum_{i=1}^{n}\left(T_{i0}d_i\right) + K_s^{\theta}\theta_r \quad (8)$$

where $K_s^{\theta} = \sum_{i=1}^{n}\left[d_i k_{si}\left(d_i - \frac{\sum_{i=1}^{n}\left(k_{si}d_i\right)}{\sum_{i=1}^{n}k_{si} + k_b}\right)\right]$ denotes the post gap-opening bending stiffness of the connection provided by the PT tendons.

Based on Eqs.(7) and (8), analyses were made and the results were compared with the test data. Fig.16 shows that the analytical results match the test data reasonably well. The analytical results, however, provide a better prediction for upward loading ($\theta_r > 0$) than for downward loading, which may be due to an asymmetrical arrangement of tendons in the specimens due to construction errors. Since the beam is not rigid; there is a small rotation due to local deformation at the center of rotation at the top and bottom of the beam before the moment reaches M_{IGO}(i.e., θ_r was not zero at M_{IGO}). M_{IGO} and the post gap-opening bending stiffness are in good agreement with the test results. Similar to previous tests (Wolski et al. 2009), there is a stiffness reduction during load reversal, which is considered to be mainly due to the flexibility of the steel channels. However, to simplify the analysis, the analytical model does not consider this effect.

Potential Improvements

Based on the results presented above, several improvements to the SCPC connection were considered. For example, as shown in Test 14, the spiral hoops may be left out to facilitate construction. The connection between the channels and the column could be a bolted connection to avoid field welding and the observed cracks at the weld toes. The four PT strands near the corners can be replaced by a bundle of PT strands at the center of the beam to simplify construction. Other friction materials could be

Journal of Structural Engineering. Submitted May 24, 2011; accepted September 6, 2012;
posted ahead of print September 8, 2012. doi:10.1061/(ASCE)ST.1943-541X.0000718

used to replace the brass plate so as to obtain equivalent or better friction performance with lower material costs.

Conclusions

A novel self-centering beam-column connection for prestressed concrete frames was developed and the behavior of the connection under cyclic loading was investigated, with the following conclusions:

(1) The proposed SCPC connection enables dry jointed construction of post-tensioned precast concrete frames with desirable self-centering behavior that surpasses traditional cast-in-place construction. The test specimens underwent a maximum relative rotation of 0.038 rad without significant damage to the beams or columns. Compared to a previous post-tensioned precast concrete beam-column connection (El-Sheikh et al 1999), the SCPC connection with a web friction device had significantly increased energy dissipation. The steel jacket not only works as part of the friction device, but also improves the behavior of the concrete, by avoiding spalling under local compressive forces.

(2) Experimental and analytical results show that the $M-\theta_r$ behavior of the SCPC connection with web friction device has a double-flag shape. An analytical model for the $M-\theta_r$ behavior of the beam-column test specimens was presented. Good agreement is observed between the experimental and analytical results.

(3) The experimental results show that the energy dissipation capacity was directly influenced by the magnitude of the friction bolt forces; while the magnitude of the initial tendon forces affects the self-centering behavior, imminent gap opening moment capacity, and initial stiffness of the connection.

Acknowledgments

This work is supported by the National Natural Science Foundation of China under Grant No.51078075, which involves Southeast University in China, and Lehigh University and San Francisco State University

in USA. In addition, the financial support from the State Key Lab of Subtropical Building Science, South China University of Technology under Grant No. 2010KB05 and a project funded by the Priority Academic Program Development of Jiangsu Higher Education Institutions are gratefully acknowledged.

References

ACI Innovation Task Group 1. (2001). Acceptance criteria for moment frames based on structural testing (T1.1–01) and commentary (T1.1R-01), American Concrete Institute, Farmington Hills, Mich.

CECS28:90. (1990). "Specification for design and construction of concrete-filled steel tubular structures." *China Association for Engineering Construction Standardization*, Beijing (in Chinese).

Chopra, A. K. (2001). *Dynamics of structures - theory and application to earthquake engineering*. 2nd Edition, Prentice Hall, Upper Saddle Rive, NJ.

Chou, C. C., Chen, J. H., Chen, Y. C., and Tsai, K. C. (2006). "Evaluating performance of post-tensioned steel connections with strands and reduced flange plates." *Earthquake Eng. Struct.Dyn.*, 35(9), 1167-1185.

Chou, C. C., and Lai Y. J. (2009). "Post-tensioned self-centering moment connections with beam bottom flange energy dissipators." *J. Constr. Steel Res*., 65(10-11), 1931-1941.

Christopoulos, C., Filiatrault, A., Uang, C. M., and Folz, B. (2002). "Posttensioned energy dissipating connections for moment-resisting steel frames." *J. Struct. Eng.*, 128(9), 1111-1120.

Dolan, C., Stanton, J., and Anderson, R. (1987). "Moment resistant connections and simple connections." *PCI J.*, 32(2), 62–74.

El-Sheikh, M., Sause, R., Pessiki S., and Lu, L. W. (1999). "Seismic behavior and design of unbonded post-tensioned precast concrete frames." *PCI J.*, 44(3), 54-71.

Englekirk, R. (2002). "Design-construction of the Paramount - A39-story precast prestressed concrete

apartment building." *PCI J.*, 47(4), 56-71.

Federal Emergency Management Agency (FEMA). (2003). "NEHRP recommended provisions for seismic regulations for new buildings and other structures. Part 1—Provisions and Part 2—Commentary." *FEMA 450*, Washington, D.C.

fib Bulletin 27. (2003). "Seismic design of precast concrete building structures: state-of-art report." *International Federation for Structural Concrete (fib)*, Switzerland.

Garlock, M. M., Ricles, J. M., and Sause, R. (2005). "Experimental Studies of Full-Scale Post-Tensioned Steel Connections." *J. Struct. Eng.*, 131 (3), 438-448.

GB 50010-2002. (2002). "Code for design of concrete structures." Chinese code, Beijing, China (in Chinese).

Korkmaza, H. H., and Tankutb, T. (2005). "Performance of a precast concrete beam-to-beam connection subject to reversed cyclic loading." *Eng. Struct.*, 27(9), 1392-1407.

Lin, Y. C., Ricles, J. M. and Sause, R. (2009). "Earthquake simulations on self-centering steel moment resisting frame with web friction devices." *Proceedings of the ASCE Structures Congress*, April 29-May 2, 2009, Austin, Texas.

Liu, B. K., Tian, J. F., Zhang, Y. Z., Xu, Y. Z., and Chang, X. F. (2007). "Behavior of ductility and energy dissipation of prestressed precast concrete frame under low-cyclic reversed loading." *Journal of Building Structures*, 28(3), 74-81(in Chinese).

Martin, L. D., and Perry, C. J. (2004). "PCI design handbook: precast and prestressed concrete." 6th Edition, *PCI*, Illinois.

Morgen, B. G., and Kurama, Y. C. (2008). "Seismic response evaluation of posttensioned precast concrete frames with friction dampers." *J. Struct. Eng.*, 134(1), 132-145.

Journal of Structural Engineering. Submitted May 24, 2011; accepted September 6, 2012;
posted ahead of print September 8, 2012. doi:10.1061/(ASCE)ST.1943-541X.0000718

Priestley, M., and MacRae, G. (1996). "Seismic tests of precast beam-to-column joint subassemblages with unbonded tendons." *PCI J.*, 41(1), 64-81.

Ricles, J. M., Sause, R., and Garlock, M. M. (2001). "Posttensioned seismic-resistant connections for steel frames." *J. Struct. Eng.*, 127(2), 113-121.

Rojas, P., Ricles, J. M., and Sause, R. (2005). "Seismic performance of post-tensioned steel moment resisting frames with friction devices." *J. Struct. Eng.*, 131(4), 529-540.

Seo, C. Y., and Sause, R. (2005). "Ductility demands on self-centering systems under earthquake loading." *ACI Struct. J.*, 102(2), 275–285.

Sucuoglu, H. (1995). "Inelastic seismic response of precast concrete frames with constructed plastic hinges." *Comput. Struct.*, 56(1), 121-131.

Wolski, M., Ricles, J. M., and Sause, R. (2009). "Experimental study of self-centering beam-column connection with bottom flange friction device." *J. Struct. Eng.*, 134 (5), 479-488.

Journal of Structural Engineering. Submitted May 24, 2011; accepted September 6, 2012;
posted ahead of print September 8, 2012. doi:10.1061/(ASCE)ST.1943-541X.0000718

Figure captions list

Fig.1 Configuration of SCPC beam-column connection with web friction device

Fig.2 Free-body diagram of SCPC connection

Fig.3 Conceptual $M-\theta_r$ behavior

Fig.4 Configuration of specimen SCPC1 (dimensions in millimeters)

Fig.5 Test setup and instrumentation

Fig.6 Hysteretic behavior in Test 2 and Test 5

Fig.7 Hysteretic behavior in Test 4 and Test 10

Fig.8 Influence of tendon forces on hysteretic behavior

Fig.9 Relationship of tendon force and relative rotation

Fig.10 Moment-relative rotation relationship of specimens without steel jacket (Test 11A)

Fig.11 Strain measurements on steel jacket

Fig.12 Hysteretic behavior in Test 14

Fig.13 Anchorage of the embedded steel plate in column (cross section view)

Fig.14 Damage in specimens after tests

Fig.15 Elongation of tendons in tested specimens as gap-opening occurs

Fig.16 Comparison of analytical and experimental $M-\theta_r$ relations

Fig.1

Journal of Structural Engineering. Submitted May 24, 2011; accepted September 6, 2012;
posted ahead of print September 8, 2012. doi:10.1061/(ASCE)ST.1943-541X.0000718

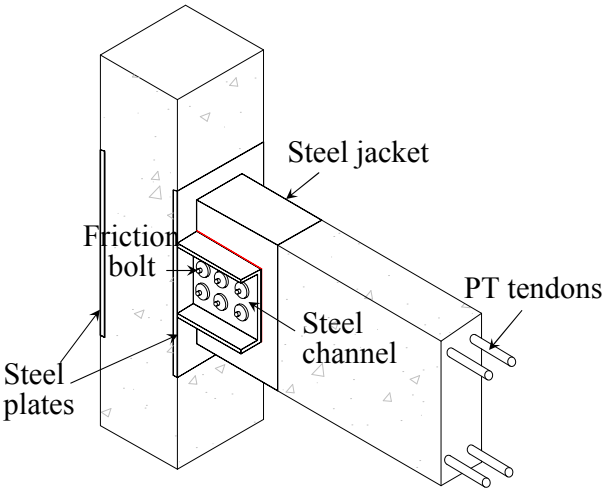

(a) 3D view

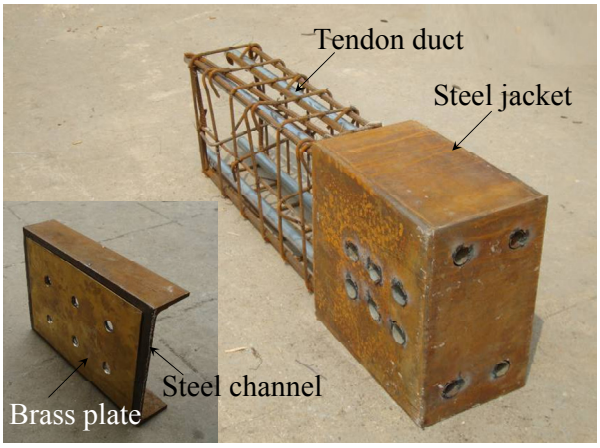

(b) Steel jacket and steel channel

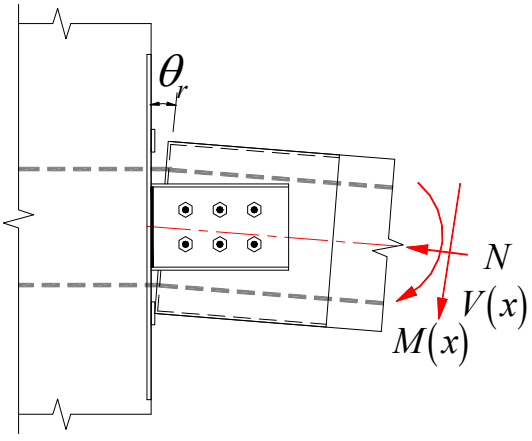

(c) Gap-opening at beam-column interface

Fig.1. Configuration of SCPC beam-column connection with web friction device

Fig.2

Journal of Structural Engineering. Submitted May 24, 2011; accepted September 6, 2012;
posted ahead of print September 8, 2012. doi:10.1061/(ASCE)ST.1943-541X.0000718

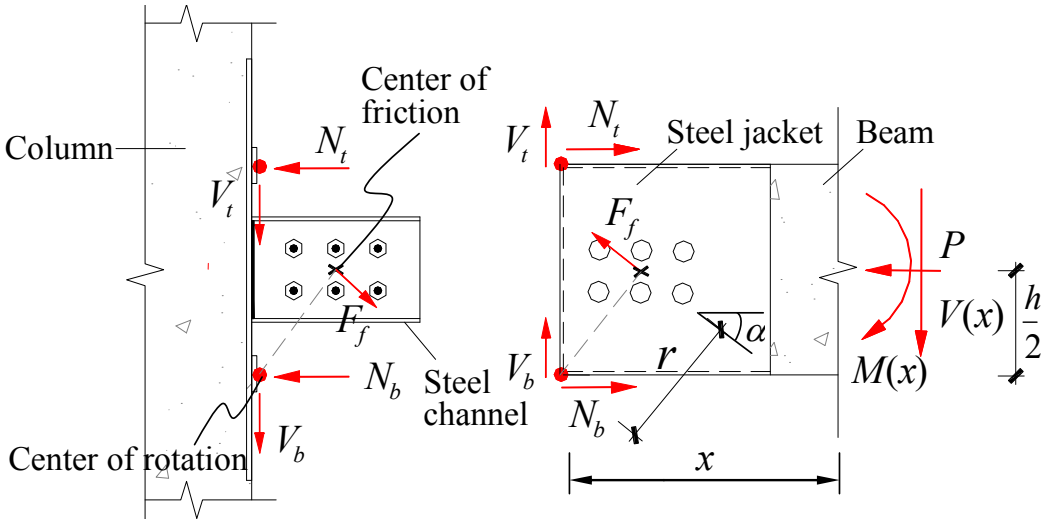

Fig. 2. Free-body diagram of SCPC connection

Fig.3

Journal of Structural Engineering. Submitted May 24, 2011; accepted September 6, 2012;
posted ahead of print September 8, 2012. doi:10.1061/(ASCE)ST.1943-541X.0000718

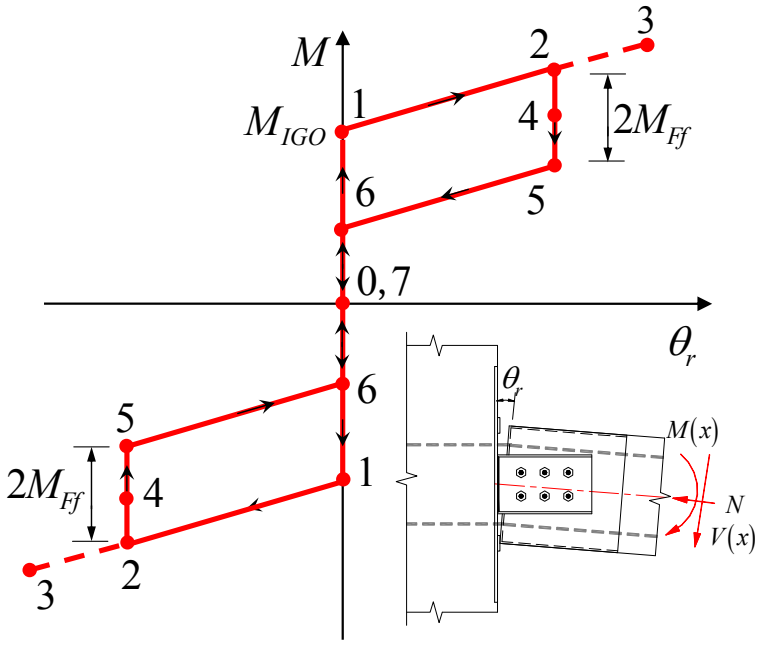

Fig. 3. Conceptual $M - \theta_r$ behavior

Fig.4

Journal of Structural Engineering. Submitted May 24, 2011; accepted September 6, 2012;
posted ahead of print September 8, 2012. doi:10.1061/(ASCE)ST.1943-541X.0000718

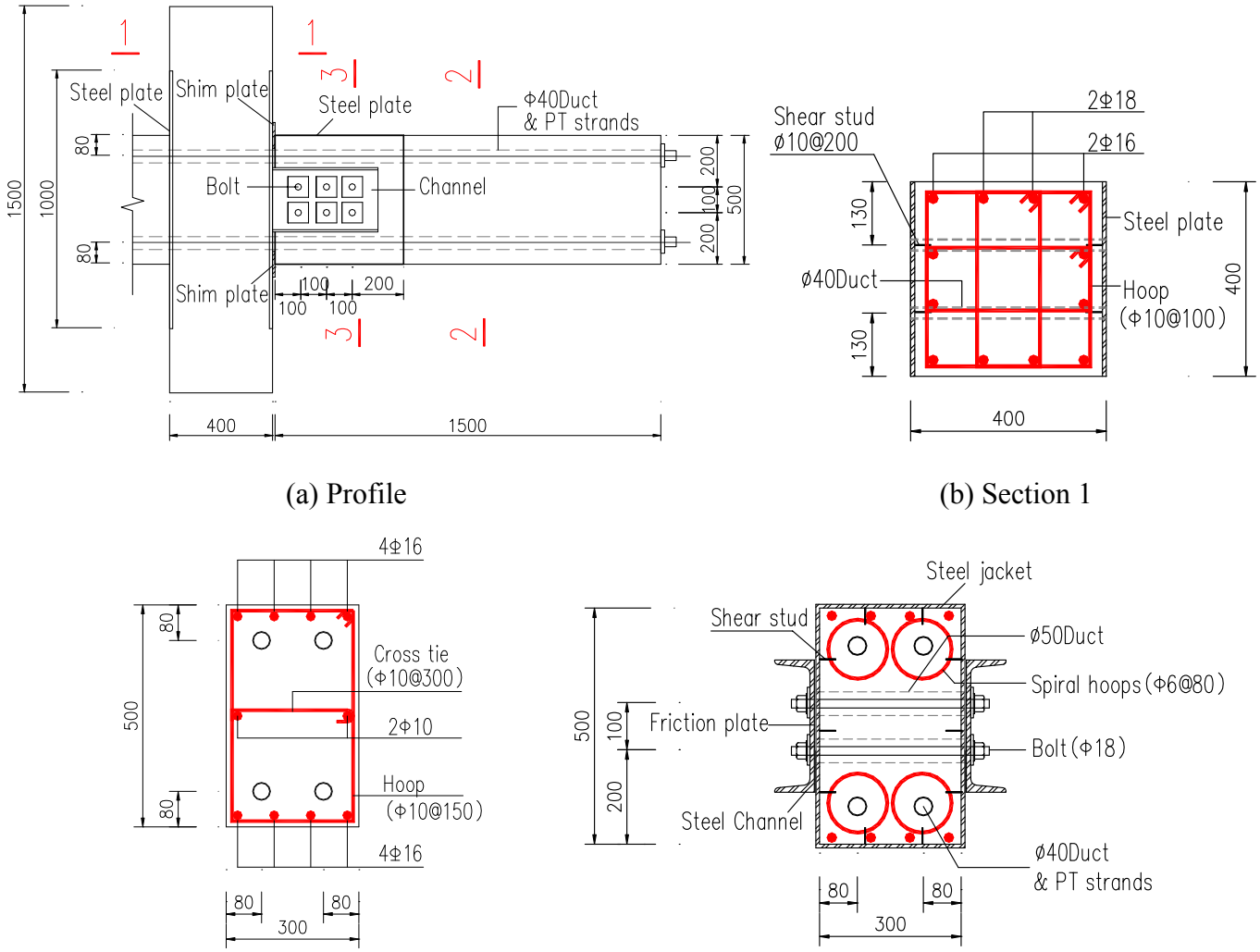

(a) Profile (b) Section 1

(c) Section 2 (d) Section 3

Fig.4. Configuration of specimen SCPC1 (dimensions in millimeters)

Fig.5

Journal of Structural Engineering. Submitted May 24, 2011; accepted September 6, 2012;
posted ahead of print September 8, 2012. doi:10.1061/(ASCE)ST.1943-541X.0000718

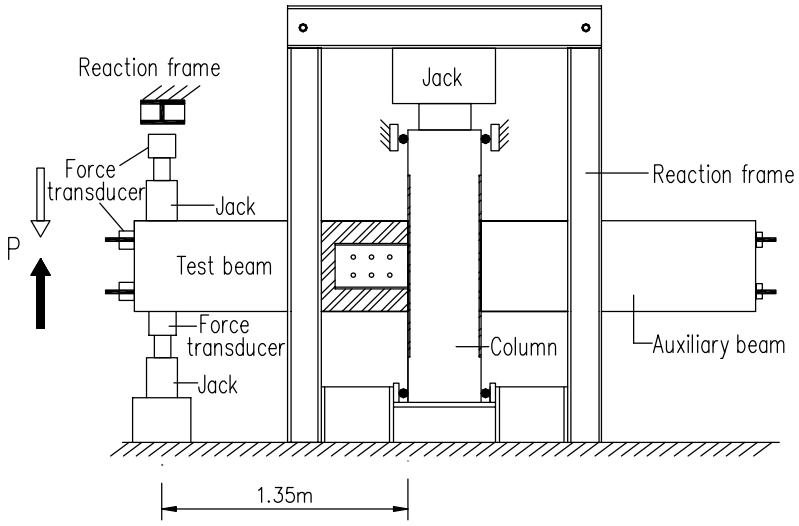

(a) Test setup

(b) Assembly during test

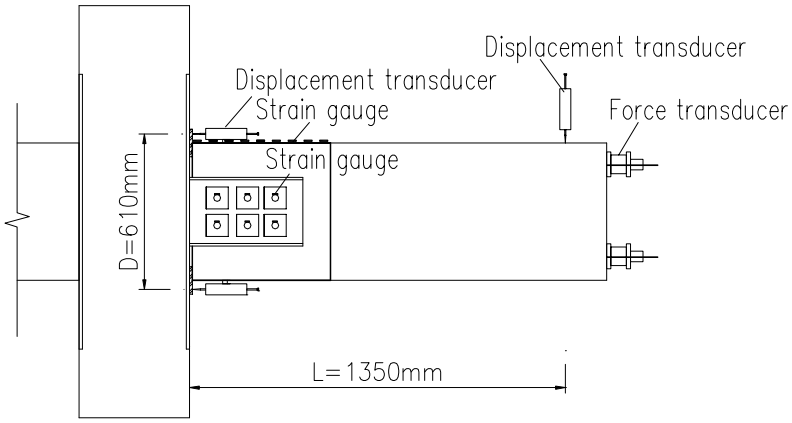

(c) Layout of gauges and sensors

Fig.5. Test setup and instrumentation

Fig.6

Journal of Structural Engineering. Submitted May 24, 2011; accepted September 6, 2012;
posted ahead of print September 8, 2012. doi:10.1061/(ASCE)ST.1943-541X.0000718

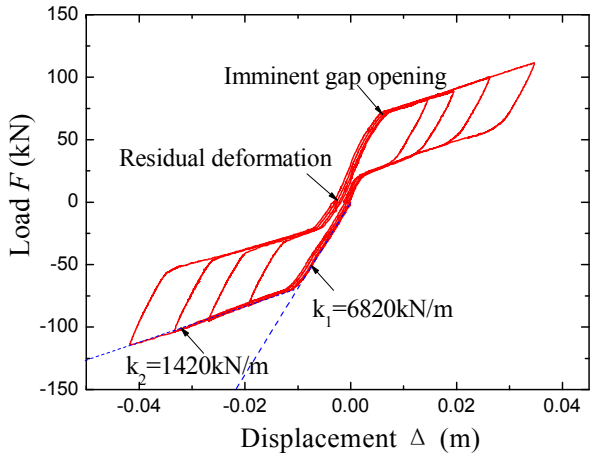

(a) $F-\Delta$ relationship (Test 2)

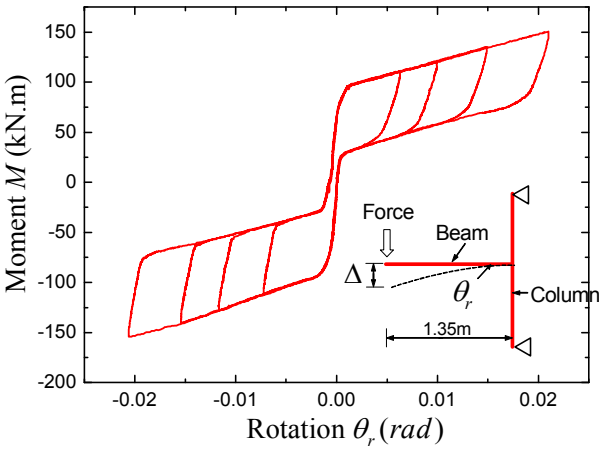

(b) $M-\theta_r$ relationship (Test 2)

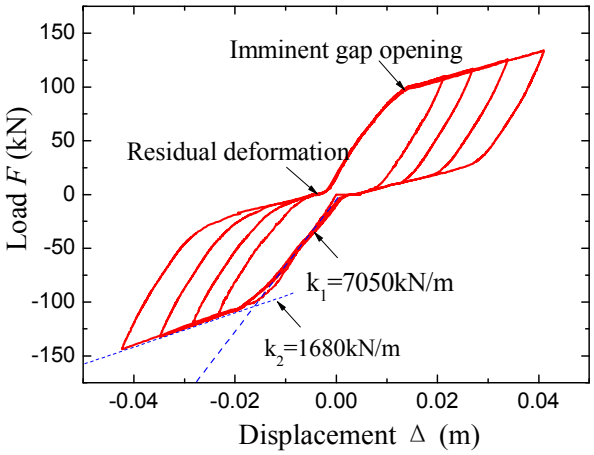

(c) $F-\Delta$ relationship (Test 5)

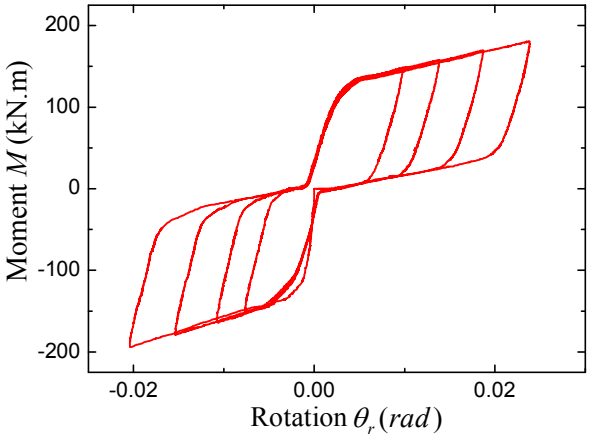

(d) $M-\theta_r$ relationship (Test 5)

Fig.6. Hysteretic behavior in Test 2 and Test 5

Fig.7

Journal of Structural Engineering. Submitted May 24, 2011; accepted September 6, 2012;
posted ahead of print September 8, 2012. doi:10.1061/(ASCE)ST.1943-541X.0000718

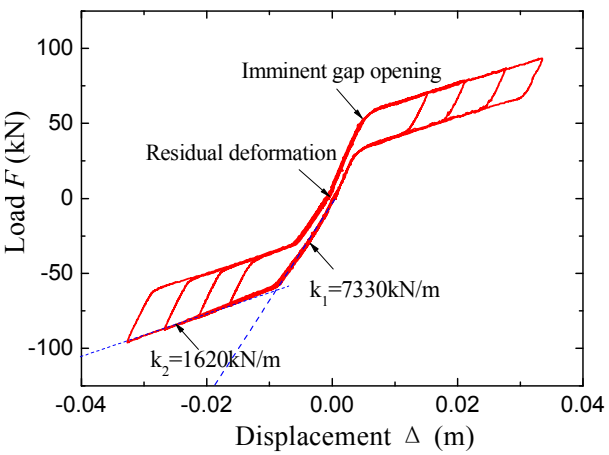

(a) $F-\Delta$ relationship (Test 4)

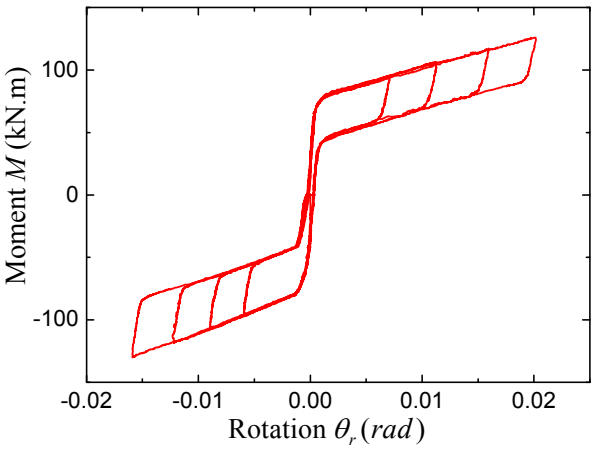

(b) $M-\theta_r$ relationship (Test 4)

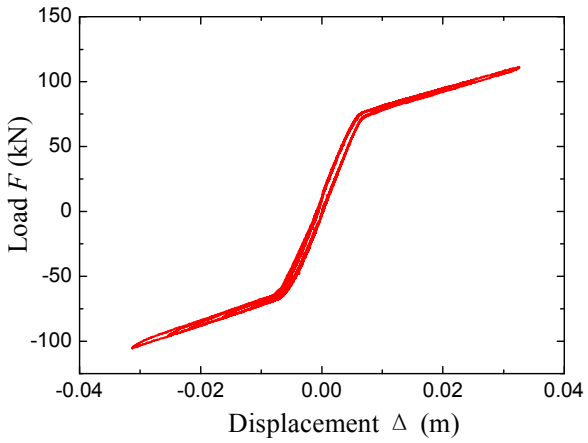

(c) $F-\Delta$ relationship (Test 10)

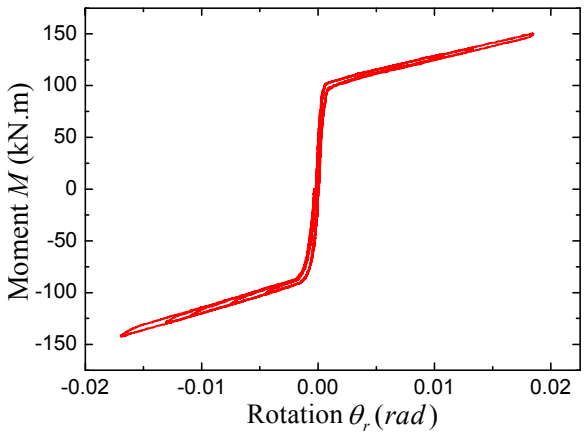

(d) $M-\theta_r$ relationship (Test 10)

Fig.7. Hysteretic behavior in Test 4 and Test 10

Fig.8

Journal of Structural Engineering. Submitted May 24, 2011; accepted September 6, 2012;
posted ahead of print September 8, 2012. doi:10.1061/(ASCE)ST.1943-541X.0000718

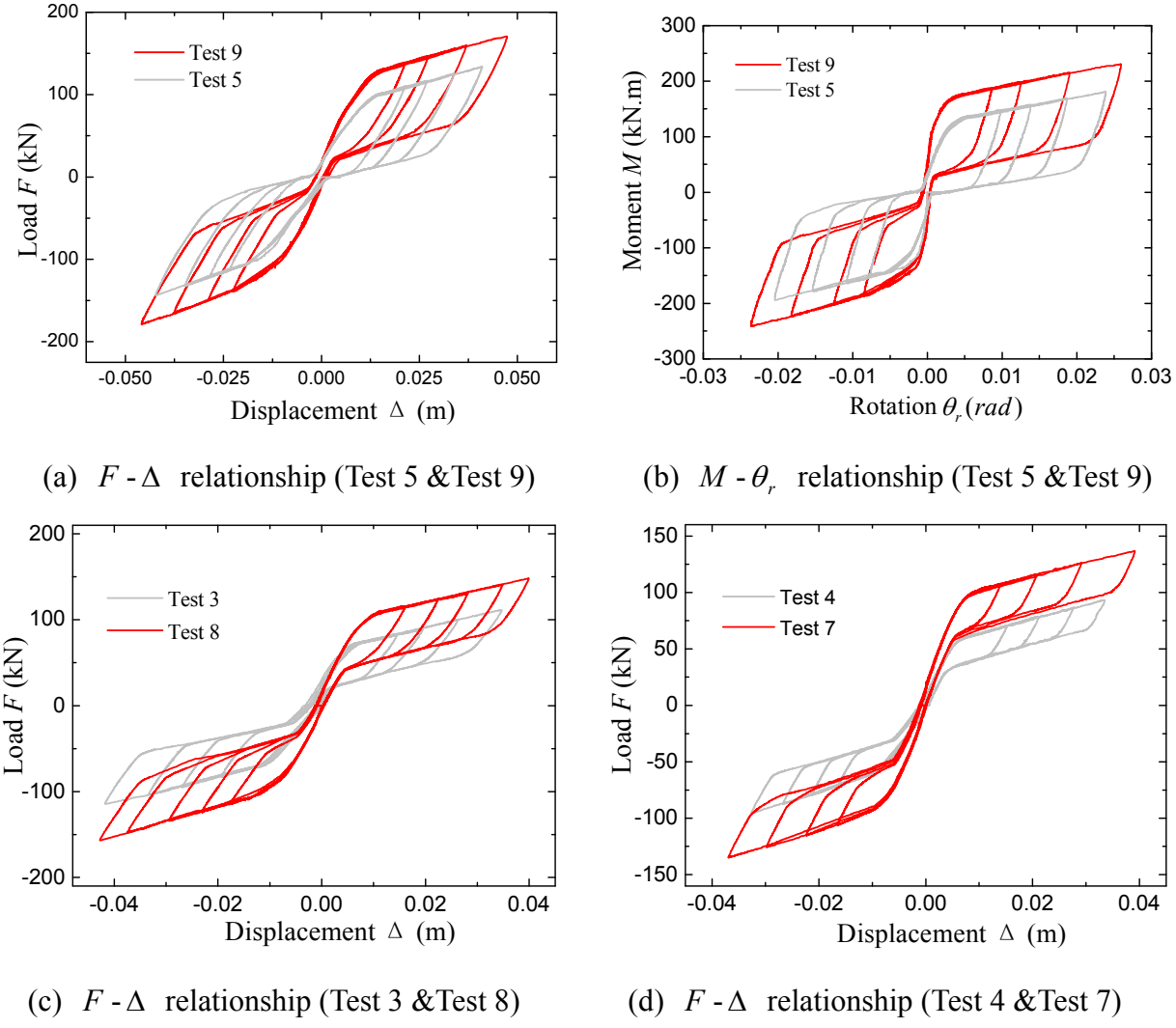

(a) F - Δ relationship (Test 5 &Test 9)

(b) M - θ_r relationship (Test 5 &Test 9)

(c) F - Δ relationship (Test 3 &Test 8)

(d) F - Δ relationship (Test 4 &Test 7)

Fig.8. Influence of tendon forces on hysteretic behavior

Fig.9

Journal of Structural Engineering. Submitted May 24, 2011; accepted September 6, 2012;
posted ahead of print September 8, 2012. doi:10.1061/(ASCE)ST.1943-541X.0000718

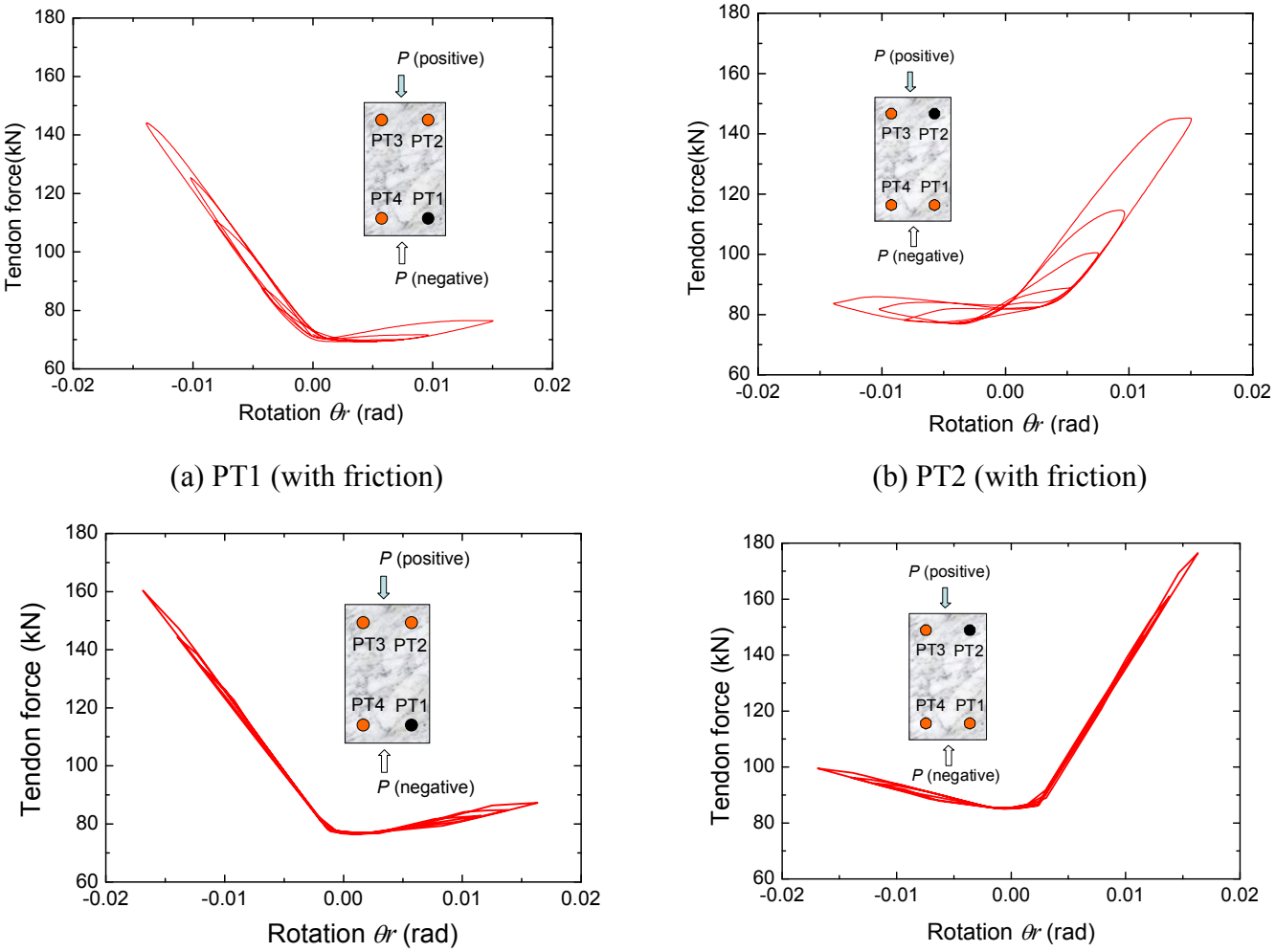

(a) PT1 (with friction)

(b) PT2 (with friction)

(c) PT1 (without friction)

(d) PT2 (without friction)

Fig.9. Relationship of tendon force and relative rotation

Fig.10

Journal of Structural Engineering. Submitted May 24, 2011; accepted September 6, 2012;
posted ahead of print September 8, 2012. doi:10.1061/(ASCE)ST.1943-541X.0000718

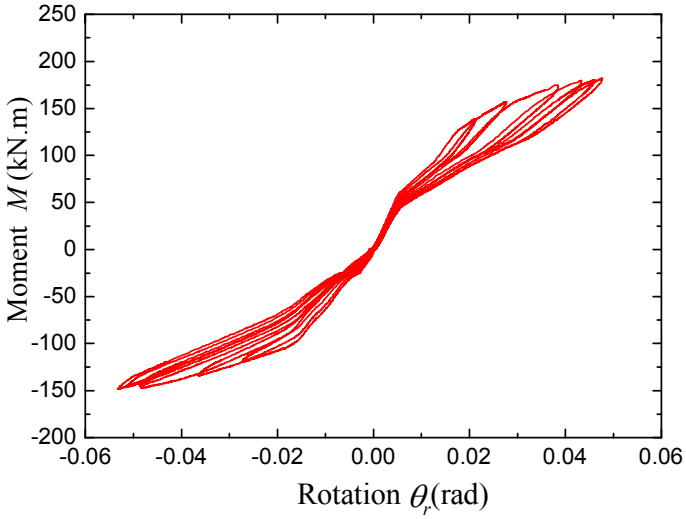

Fig.10. Moment-relative rotation relationship of specimens without steel jacket (Test 11A)

Fig.11

Journal of Structural Engineering. Submitted May 24, 2011; accepted September 6, 2012;
posted ahead of print September 8, 2012. doi:10.1061/(ASCE)ST.1943-541X.0000718

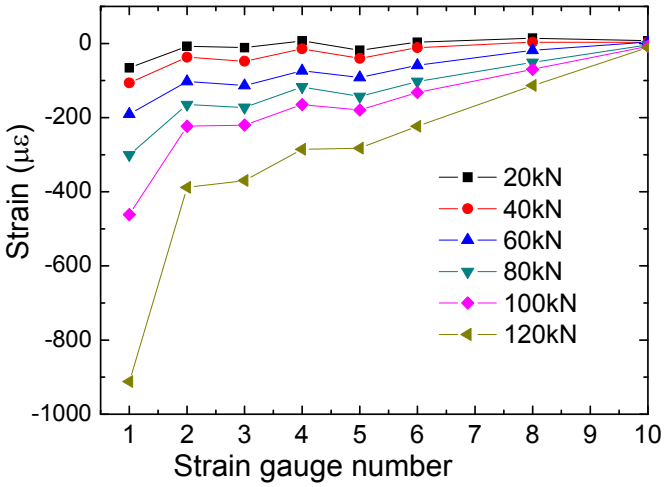

(a) Strains during upward loading

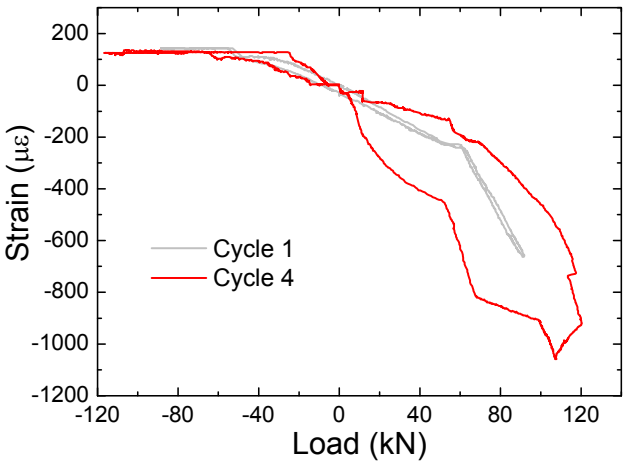

(b) Strain-load response (gauge 1)

Fig.11. Strain measurements on steel jacket

Fig.12

Journal of Structural Engineering. Submitted May 24, 2011; accepted September 6, 2012;
posted ahead of print September 8, 2012. doi:10.1061/(ASCE)ST.1943-541X.0000718

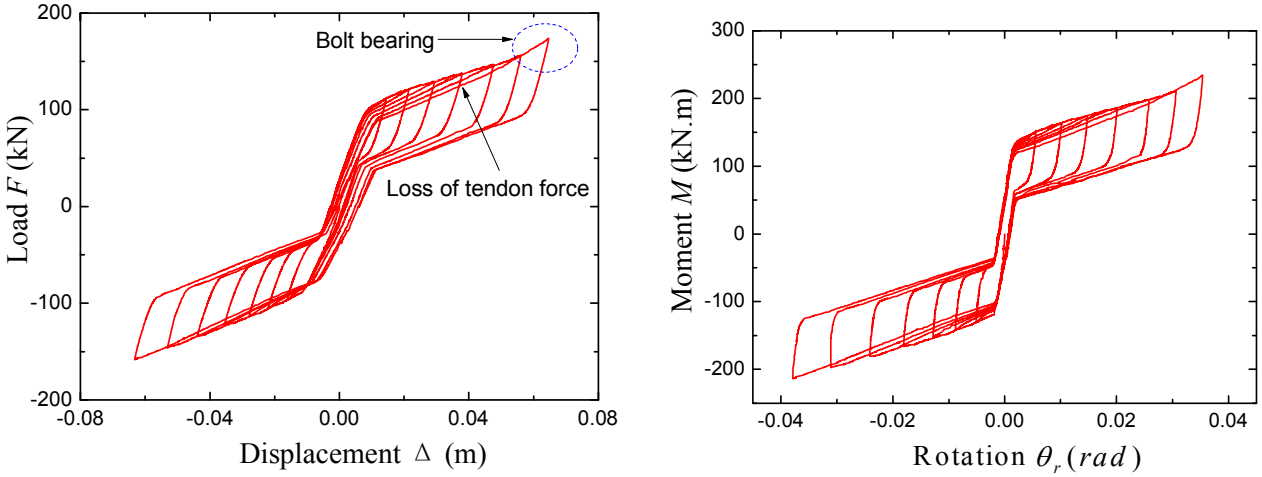

(a) F - Δ relationship (b) M - θ_r relationship

Fig.12. Hysteretic behavior in Test 14

Fig.13

Journal of Structural Engineering. Submitted May 24, 2011; accepted September 6, 2012;
posted ahead of print September 8, 2012. doi:10.1061/(ASCE)ST.1943-541X.0000718

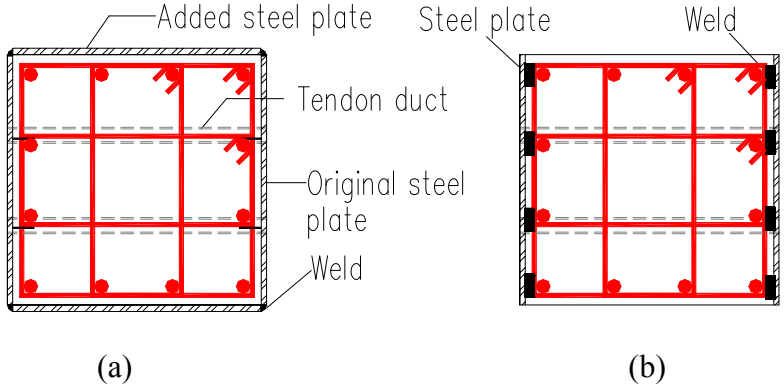

Fig.13. Anchorage of the embedded steel plate in column (cross section view)

Fig.14

Journal of Structural Engineering. Submitted May 24, 2011; accepted September 6, 2012;
posted ahead of print September 8, 2012. doi:10.1061/(ASCE)ST.1943-541X.0000718

(a) XJ1 (after Test 12) (b) SCPC2 (after Test 11A) (c) SCPC1 (after Test 9)

Fig.14. Damage in specimens after tests

Fig.15

Journal of Structural Engineering. Submitted May 24, 2011; accepted September 6, 2012;
posted ahead of print September 8, 2012. doi:10.1061/(ASCE)ST.1943-541X.0000718

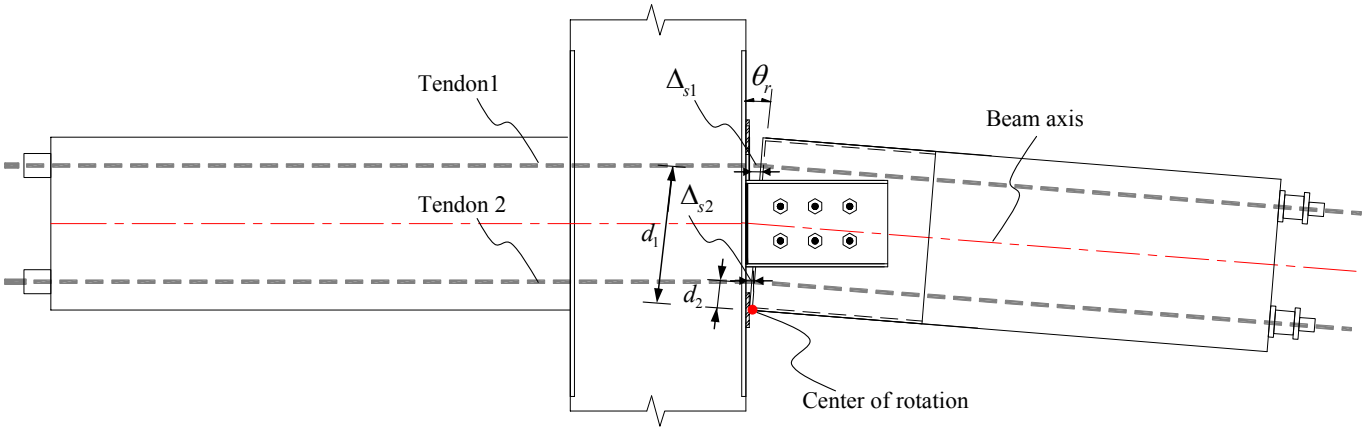

Fig.15. Elongation of tendons in tested specimens as gap-opening occurs

Fig.16

Journal of Structural Engineering. Submitted May 24, 2011; accepted September 6, 2012;
posted ahead of print September 8, 2012. doi:10.1061/(ASCE)ST.1943-541X.0000718

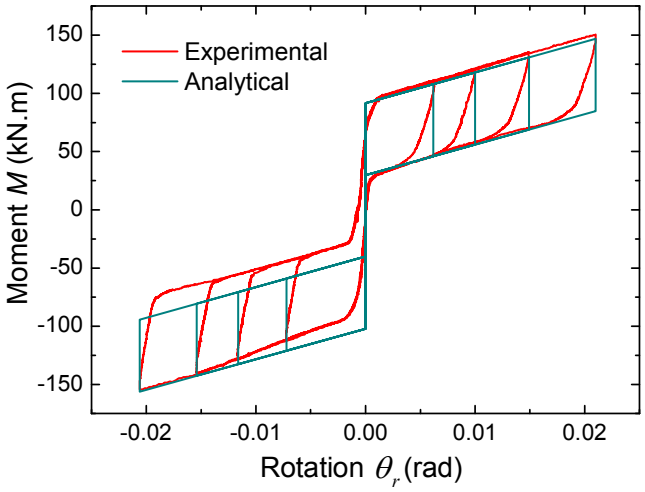

(a) Test 2

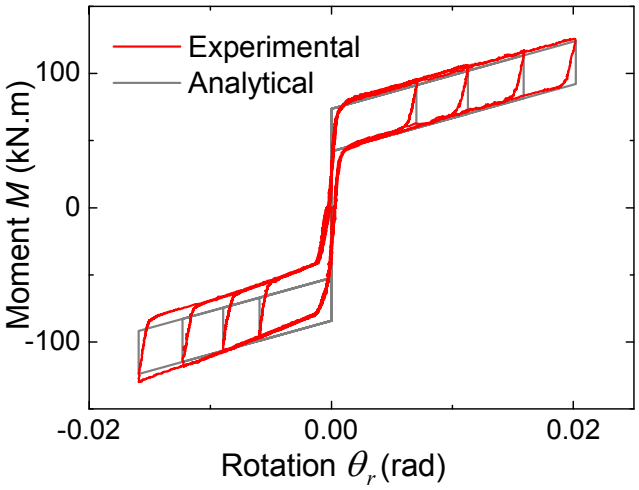

(b) Test 4

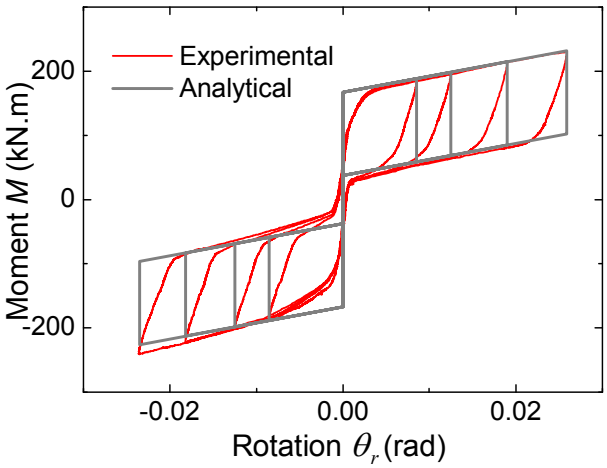

(c) Test 9

Fig.16. Comparison of analytical and experimental $M - \theta_r$ relations

Journal of Structural Engineering. Submitted May 24, 2011; accepted September 6, 2012;
posted ahead of print September 8, 2012. doi:10.1061/(ASCE)ST.1943-541X.0000718

Table 1. Test matrix

Test number	Specimen denotation	F_0 (kN)	R_0	N_0 (kN)	Characteristics of test
1	SCPC1	289	0.34	180	Trial test (with friction device)
2	SCPC1	274	0.33	90	Medium friction force
3	SCPC1	274	0.33	150	Higher friction force
4	SCPC1	270	0.32	45	Low friction force
5	SCPC1	269	0.32	180	High friction force
6	SCPC1	303	0.36	90	Relationship of tendon forces and relative rotation
7	SCPC1	482	0.57	45	High PT force, low friction force
8	SCPC1	446	0.53	90	High PT force, medium friction force
9	SCPC1	446	0.53	180	High PT force, high friction force
10	SCPC1	443	0.53	/	No friction device
11A	SCPC2	453	0.54	/	No steel jacket, no friction device
12	XJ1	/	/	/	Monolithic cast-in-place beam-column connection
13	SCPC3	342	0.41	/	Stresses measurements on steel jacket
14	SCPC3	445	0.53	180	No spiral hoops